REVISION 1

Geochemistry of Pyrochlore minerals from the Motzfeldt Centre, South Greenland: The Mineralogy of a Syenite-Hosted Ta, Nb deposit

Jamie A. McCreath[1*], Adrian A. Finch[1†], Donald A. Herd[1], Ashlyn Armour-Brown[2]

[1]Centre for Earth Resources St Andrews (CERSA) and Department of Earth Sciences, University of St Andrews, Irvine Building, St Andrews, Fife, KY16 9AL, UK.

[2]Angus and Ross plc, Kirkbymoorside, York, UK.

[*] Present address: Red Rock Resources plc, 115 Eastbourne Mews, London W2 6LQ, UK.

[†] Corresponding author, email: adrian.finch@st-andrews.ac.uk

Keywords: pyrochlore, tantalum, alkaline, Gardar Province, hydrothermal alteration, Greenland

ABSTRACT

Pyrochlore minerals are a common accessory phase in the syenite and nepheline syenite rocks of the Motzfeldt alkaline centre, Gardar Province, South Greenland, and are of important economic interest due to their exceptional ability to host a variety of high field strength elements. In this study pyrochlore from two distinct intrusive units within the Motzfeldt centre have been studied. The largely homogeneous syenite and nepheline syenite rocks of the Flinks Dal formation host oscillatory and sector zoned pyrochlore, which have experienced minor alteration in the presence of high temperature, dominantly juvenile magmatic fluids. Alteration is characterised by variable decrease in the Na, Ca and F contents and addition of Sr and K, accompanied by introduction of *A* and *Y* site vacancies. Pyrochlore from the more heterogeneous and intensely altered syenite rocks of the Motzfeldt Sø Formation are pervasively altered through interaction with lower temperature

evolved hydrothermal fluids. During this phase of alteration cations are preferentially leached from the A and Y sites, accompanied by progressively increasing hydration. In both formations the proportion of B-site cations remains unaltered regardless of the degree of alteration. The alteration encoded in the pyrochlores of the Motzfeldt centre records the different hydrothermal conditions the two formations experienced during the subsolidus, showing how evolution of fluids within one intrusive unit can vary both spatially and temporally.

KEYWORDS: Gardar Province, Alkaline Rocks, High Field Strength Elements, Tantalum

INTRODUCTION

There is worldwide interest in the discovery and extraction of high field strength elements (HFSE, such as Zr, Hf, Nb, Ta) for applications in the electronics industry. Many commercially viable deposits are hosted by pyrochlore supergroup minerals because the pyrochlore structure accommodates a variety of large, high field-strength ions, hence the mineralogy and geochemistry of pyrochlore is of widespread commercial and academic interest. The present article considers pyrochlore minerals from the Motzfeldt centre, part of the Gardar province, South Greenland. The Motzfeldt area is estimated as one of the world's largest Ta deposits; conservative estimates suggest a potential for over 500 million tons of ore, containing over 1400 ppm Nb, 120 ppm Ta and 60 ppm U. Masses of 30 Mt with a potential for >250 ppm Ta have been suggested by targeting facies of syenite hosting the highest modal abundance of pyrochlore (Thomassen 1988; Armour-Brown 2001). We consider the mineralogy, petrology and petrogenesis of these pyrochlores and their host rocks to understand more fully the nature of this exceptional Ta deposit. In doing do, we provide a detailed characterisation of pyrochlore in a most important commercial setting.

GEOLOGICAL SETTING OF THE MOTZFELDT CENTRE

Motzfeldt is one of four major alkaline centres belonging to the Igaliko complex. The complex is situated in the north-east of the mid-Proterozoic Gardar province of South Greenland, representing the products of repeated rift-related alkaline magmatism during the interval ~1300-1140 Ma (Blaxland *et al.* 1978; Upton & Emeleus 1987; Upton *et al.* 2003). The Motzfeldt centre (1273 ± 6 Ma, McCreath *et al.* 2012) was emplaced into Ketilidian age (1900-1700 Ma), subduction related I-type granites, belonging to the Julianehåb batholith (Allaart 1976), through a combination of block stoping, ring fracture and partial ring dyke formation (Emeleus & Harry 1970; Jones 1980). The tensional stress regimes active during the Gardar can be inferred from the orientations of faults and dykes. At the earliest rifting, tension was parallel to ENE-WSW and a series of NNW-SSE basic dykes ('the Brown Dyke 0' or BD0 swarm) resulted (Upton & Emeleus 1987). The Gardar rift soon

adopted a dominant E-W sinistral transtension generating E-W faults and *en echelon* NE-SW dilation along which most Gardar dykes were intruded (see Upton *et al.* 2003 for a review and for a map placing Motzfeldt in the context of the Gardar province). The geography of SW Greenland is now dominated by a series of deep NE-SW fjords and it is inferred that these lie along the major Gardar vertical rifting. The earliest Gardar rocks are a sequence of interbedded clastic sediments, pyroclastics and lavas together called the 'Eriksfjord formation'. From both *in situ* exposures and the widespread presence of Eriksfjord xenoliths in Gardar central complexes, it is thought that the Eriksfjord once covered the majority of SW Greenland.

The Motzfeldt Centre covers an area of approximately 150 km^2 with excellent 3-dimensional exposure in steeply dissected glacial valleys. The rocks comprise syenite, nepheline syenite, syenogabbro and minor intrusives, ranging in composition from basic to evolved rocks and quartz normative to agpaitic (Emeleus & Harry 1970, Jones 1980, Tukiainen 1988). The general structure of Motzfeldt comprises steep-sided concentric intrusions whose marginal contacts dip outwards. The roof to the intrusion was the Eriksfjord Formation, and recent glaciation in the east of the centre may have exploited the sub-horizontal plane of weakness that the roof zone provided to leave a relatively flat land surface that is consistently within a few 10s of metres from the roof. Initial mapping of Motzfeldt by Emeleus & Harry (1970) distinguished 5 major syenite and nepheline syenite units, prefixed SM and numbered 1 to 5 broadly in order of emplacement, and two main satellite syenites called the North and East Motzfeldt syenites. Jones (1980) later added an agpaitic syenite (SM6) and identified a heterogeneous facies of SM4 termed HY. Bradshaw (1985, 1988) and Tukiainen *et al.* (1984) produced a revised field description of the centre, using different terminology, dividing the centre into the Geologfjeld (GF), Motzfeldt Sø (MSF) and Flinks Dal Formations (FDF), within each of which are several subdivisions (Fig. 1). The SM1 and 3 units of Emeleus and Harry (1970) correspond to the MSF and GF; SM2, 4, 5 and 6 form the FDF. In detail the correlations between old and new nomenclatures are few. SM2 and parts of SM4 together comprise the ***FDF – Porphyritic syenite***; SM5 was subdivided into the ***FDF – Nepheline syenite***

and ***FDF – Foyaite*** (here used to mean a nepheline syenite with a well-defined lamination). HY does not appear in the new nomenclature. The earliest activity in Motzfeldt is interpreted as lying to the North and East; it comprises SM1 and SM3 of Emeleus & Harry (1970) and the GF and MSF of Bradshaw (1985, 1988). The East Motzfeldt syenite of Emeleus & Harry (1970) is now recognised as an extension of the Motzfeldt Sø Formation, offset by the Flinks Dal Fault (Fig. 1), rather than a separate satellite intrusion. Younger activity, in the middle of the centre, cored out older syenites and now forms the FDF, which comprises the middle, south and west of the complex. The youngest activity is a series of subhorizontal peralkaline sheets and syenogabbro and larvikite giant-dykes. The relative ages of these late-stage intrusives is not known although they are inferred to be part of Motzfeldt.

The area East of Motzfeldt Sø lake comprises the Geologfjeld (GF) and the Motzfeldt Sø Formations (MSF) of Bradshaw (1985, 1988). The MSF was subdivided into: ***MSF – Marginal Arfvedsonite Syenite***, ***MSF – Altered Nepheline Syenite*** and ***MSF – Nepheline Syenite***. Within the MSF are a number of late microsyenite sheets termed the ***MSF – Peralkaline Microsyenite Suite*** (Bradshaw 1988; Tukiainen 1988). SM1 corresponds to the MSF – Altered Nepheline Syenite and Marginal Arfvedsonite Syenite; SM3 broadly corresponds to the MSF – Nepheline Syenite, Alkali Syenite and Peralkaline Microsyenite Suite. The frequency and thickness of peralkaline microsyenite sheets increase towards the upper areas of the formation with associated increase in textural heterogeneity and degree of alteration. The ***GF – Nepheline Syenite*** is considered a 'fresh' variant of the MSF – Altered Nepheline Syenite which was impervious to alteration. Pervasive alteration within the Motzfeldt Centre is restricted to the MSF suggesting that the hydrothermal activity was intimately associated with this unit. The rocks to the northeast of the centre, belonging to the MSF, are the host to the Ta-rich pyrochlore and the principal focus of the present study. Unlike the units of the FDF, which are largely homogeneous syenite and nepheline syenite, units from the MSF display a high degree of textural, mineralogical and chemical heterogeneity. Rocks from the MSF display orange, highly-oxidised alkali feldspar and alteration of mafic minerals to Fe-

oxides, a feature largely absent from the FDF. The MSF has been the site of much interest since the early 1980s, when detailed mapping commenced as part of the Syduran uranium exploration project (Armour-Brown *et al.* 1983). Work by the Greenland and Denmark Geological Survey (GEUS, formerly GGU) (Tukiainen 1988; Tukiainen *et al.* 1984) revealed a number of localities containing economically interesting amounts of Nb, Ta, Th, U, Zr and REEs hosted within pyrochlore minerals.

PYROCHLORE GROUP MINERALS

Some compositional data on the pyrochlore group minerals from the MSF were presented by Tukiainen (1988) although no petrographic relationships or petrogenetic implications were inferred. Pyrochlore is a complex mineral system because of a combination of extraordinary geochemical variability and widespread non-stoichiometry. They can be expressed by the general formula $A_{2-m}B_2X_{6-w}Y_{1-n}$, where *A* represents large cations in eight-fold (cubic) coordination, usually Na, Ca, Mn, Fe^{2+}, Sr, Cs, Ba, rare earth elements (REEs = Yttrium and lanthanides), Pb, Bi, Th, U, water or site vacancies. The *B*-site is occupied by smaller cations in six-fold (octahedral) coordination, typically Al, Nb, Ta, Ti, Fe^{3+}, Zr and Sn. *X* is typically O but can also include OH^- and F. *Y* is occupied by F, O, OH^-, water or site vacancies (Chakoumakos 1984; Hogarth 1977; Lumpkin & Ewing 1995; Atencio *et al.* 2010). The symbols *m*, *w* and *n* represent parameters indicating incomplete occupancy of the A, X and Y sites, respectively. The values of *m* range between 0-2, *w*=0-0.7 and *n*=0-1 (Atencio *et al.* 2010). Classification of pyrochlore minerals is based on the International Mineralogical Association (IMA) scheme of Hogarth (1977, modified by Atencio *et al.* 2010), which defined groups based on the atomic proportion of the major *B*-site cations, including Nb, Ta and Ti. Within each group individual species are defined with respect to the atomic proportion of *A*-site cations (Hogarth 1977, Atencio *et al.* 2010).

Many pyrochlores show enrichment of large cations including Pb^{2+}, Ba^{2+} and K^+. The incorporation of these large ions into the pyrochlore structure is problematic since their ionic radii (1.18, 1.36 and

1.38 Å respectively, in octahedral co-ordination) makes accommodation in the *A* and *B* sites difficult. They may be accommodated through significant structural distortions and coupled substitutions involving vacancy formation but this would modify the overall stoichiometry. Hogarth *et al.* (2000) suggested these large cations may be located interstitially in the Wyckoff 32e site, with the modified crystal structure resembling B_2O_6Z with *Z* occupied by the larger cation. Relatively high amounts of silica (up to ~10 wt%) are also reported from altered pyrochlore group minerals (Johan & Johan 1994), yet its structural role remains unclear. Hogarth (1977) suggested that high silicon contents are due to microcrystalline impurities of other silicate minerals, while Voloshin *et al.* (1989) proposed that high silicon content results from Si in an 'amorphous state'. Bonazzi *et al.* (2006) suggest that 30-50% of silica detected by EPMA may be in octahedral coordination in the *B*-site, whereas a larger fraction of 50-70% silicon is concentrated in radiation-damaged crystal domains (Bonazzi *et al.* 2006). Octahedral silicon [$Si(OH)_6$] at room pressure is known in thaumasite (ideal structure $Ca_3[Si(OH)_6](SO_4)(CO_3)\cdot 12H_2O$) (Edge and Taylor 1969), however six-coordinate silicon is largely restricted to high pressure minerals such as stishovite (Finger & Hazen 1991; Ross *et al.* 1990). Luca *et al.* (2005) suggested that Si can be hosted within hexagonal channels running parallel to the c-axis of a defect pyrochlore structure as separate SiO_4 tetrahedra.

Significant hydration is also associated with alteration in natural pyrochlore. In pyrochlore from nepheline syenite, Lumpkin & Ewing (1995) inferred H_2O contents by the difference of the analytical totals by Electron Probe MicroAnalysis (EPMA) from 100%, to range from 2 to 14 wt% depending on the type and degree of alteration.

SAMPLE PREPARATION AND ANALYTICAL TECHNIQUES

Samples for the present study were collected during field seasons in Greenland during the summers of 2005 and 2006. In addition, material from cores collected by Angus and Ross plc were also sampled. Sample reference numbers refer to the collections of the University of St Andrews, UK and sample locations (latitude and longitude) can be found in McCreath (2009). Fieldwork focussed

157 on the areas to the N and E of Motzfeldt Sø and the samples in the present study derive from the
158 MSF – Altered Nepheline Syenite unit in locations '1', '4' and '5' (Fig. 1). The location numbers
159 derive from target areas identified by Angus and Ross plc.

160 Rocks from the MSF and FDF were analysed as polished thin sections and pyrochlore mineral
161 separates hand-picked under a binocular microscope and mounted on polished epoxy blocks. Using
162 X-ray diffraction, the pyrochlore separates are single-phase with significant line-broadening. We
163 infer that the pyrochlores are partly, but not entirely, amorphous. This is consistent with the critical
164 dose curves using the data of Lumpkin & Ewing (1988) for pyrochlores of this age and U/Th
165 concentrations (Tables 1, 2). Electron microscopy and electron probe microanalyses (EPMA) were
166 performed in the Department of Earth Sciences at the University of St Andrews using a Jeol JXA
167 8200 Superprobe. A SAMx Energy Dispersive System (EDS) was used to obtain qualitative
168 estimates of mineral compositions prior to quantitative analysis, particularly to ensure that all
169 significant elements were present in WDS analytical programs. A 22 element program was used
170 with the electron beam operating at an accelerating voltage of 20 kV, a beam current of 30 nA with
171 a spot diameter of 1-2 μm. Count times were 60 s on peak and 30 s on each background position.
172 Na, Mg, Al, Si, P, K, Ca, Ti and Mn were measured on the Kα emissions; Sr, Y, Zr, Nb, Sn, Ba, La,
173 Ce, Yb, Ta, W on Lα, Pr, Nd, Gd and Dy on Lβ, Pb and Th on Mα and U on the Mβ emissions. Na,
174 Mg, Al, Si and Y were measured using a TAP diffracting crystal; P, K, Ca, Ti, Sr, Y, Zr, Nb, Sn,
175 Ba, Pb, Th and U were measured on PET and all other elements were measured on LIF. Data were
176 processed using SAMx software with fully quantitative ZAF corrections to obtain final element
177 analyses. The following well-characterised natural and synthetic standards were used during
178 analyses: wollastonite (Ca), orthoclase (K), albite (Na), galena (Pb), quartz (Si), celestite (Sr),
179 zircon (Zr), rutile (Ti), MgF_2 (F), metallic Fe, Mn, Nb, Ta, Th and U, synthetic phosphates of La,
180 Ce, Pr, Nd, Sm, Gd and Dy. Typical precisions using the instrument are ± 0.2 wt%. Back-scattered
181 electron (BSE) images were acquired on the same instrument using an accelerating voltage of 15
182 kV with beam current of 20 nA to ensure a sharp image. Precision of compositional data to 95%

confidence interval vary from element to element but are typically ~0.03 wt.%. Sample images were processed using SAMx software and later enhanced using Adobe Photoshop.

All pyrochlore analyses were calculated to structural formula based on a *B*-site cation total of 2 atoms per formula unit (apfu) to allow for any *A*-site vacancies to be calculated (Hogarth 1977). The analytical precision in EPMA data correspond typically to 0.001 apfu when this data transformation is applied. One of the major problems of assigning structural formulae to EPMA data is uncertainty in the oxidation state of Fe. In the reduced state (Fe^{2+}) iron preferentially enters the *A*-site whereas Fe^{3+} preferentially enters the *B*-site. In the present study, assignment of Fe to the *B*-site in highly altered samples, where Fe is often in high quantities, would lead to Fe in both *A*- and *B*-sites since Fe concentrations are large and the *B*-site is capped at 2 apfu. Therefore Fe is reported as FeO and assumed to enter the *A*-site.

FLINKS DAL FORMATION PYROCHLORE

Textural character

Pyrochlore from the FDF are hosted by a fine to medium grain nepheline syenite, usually occurring as <80 μm euhedral to subhedral crystals disseminated throughout the rock, occasionally in clusters or crystal aggregates, and present in amounts varying from 2-10 vol.%. They are characterised by an octahedral habit and strong honey-yellow colour in transmitted light. BSE imaging of many pyrochlores reveals well developed magmatic zonation (Fig. 2) identified by their excellent concentric growth zoning (e.g. Fig. 2a, b & d) developed on a 1-5 μm scale. The majority of samples also show sector zoning (e.g. Fig. 2c).

Several pyrochlore samples from the FDF show textures that cannot be attributed to magmatic growth features. The BSE images in Figure 2e & f show pyrochlore with strong magmatic compositional zoning overprinted by irregular areas with a brighter BSE emission, which are interpreted as areas of alteration overprinting the original magmatic textures of the crystal.

Alteration penetrates the crystal in an irregular 'watermark' type texture from the crystal margin. The BSE contrast between mineral growth zones in the altered areas is less intense than in unaltered areas and has an overall brighter BSE emission, giving the altered area a washed out appearance. However, the alteration front is marked by a narrow zone with a dark BSE emission (black arrow), aiding in the identification of such features. Figure 2f shows a weak fracture (white arrow) penetrating into the crystal suggesting that alteration is to some degree fracture controlled. However many examples show no preserved or annealed fractures, and relict magmatic features, consistent with intracrystalline diffusion ('leaching') or coupled dissolution-reprecipitation as the principal controls of alteration.

Magmatic chemical zoning

Representative EPMA analyses of pyrochlore from the FDF are shown in Table 1. When plotted in the ternary Ti-Nb-Ta diagram (modified after Nickel 1992), FDF pyrochlore lies within the pyrochlore group (Fig. 3) showing Nb enrichment. The other major cations in the *A*-site are principally Na and Ca. Typical ranges for these cations are 0.020 to 0.550 atoms per formula unit (apfu) for Na and 0.620 to 1.150 apfu for Ca. The ∑REEs (La, Ce, Pr, Nd, Sm, Gd, Dy and Yb) are typically <0.06 apfu and dominated by La and Ce, which account for 65-85% of the total REE. In many samples the heavier REEs are <0.01 apfu. None of the minor *A*-site cations exceed 20% of the *A*-site total, therefore the FDF minerals are classified as members of the pyrochlore group *sensu stricto* (Hogarth 1977, Atencio *et al.* 2010).

Samples showing well developed concentric zonation were examined using EPMA on mineral traverses from core to rim, with spot analyses on each of the dominant mineral zones. Each crystal (six separate pyrochlore crystals analysed from two pyrochlore rich samples) displays strong compositional variations over each of the contrasting zones. Traverses from core to rim on all samples (Fig. 4) show a slight elevation of Ta in the core with respect to the rim. Typical Ta values are 0.06-0.08 apfu in the core decreasing steadily to 0.02-0.03 apfu in the rim although no clear

compositional variation in Ta content exists along individual zones. Compositional variation between mineral zones is most obvious in the higher valency elements; Mn^{2+}, U^{4+}, Ti^{4+} (Si^{4+} and Zr^{4+} show similar trends but are not shown in Fig. 4). Figure 4 shows that Ti, U and Mn are elevated in the bright, high-BSE zones and depleted in the dark, low-BSE zones. In contrast, the low-BSE zones display a slight elevation in the low-valency *A*-site elements, Na^{+} and Ca^{2+}, which are depleted in the high-BSE zones. Nb shows a flat profile regardless of mineral zonation. The relationship between compositional zoning and REE content is generally weak. In samples where F was analysed, we observe a strong relationship between high F content in bright-BSE zones.

Chemical effects of alteration

Several FDF pyrochlore samples show evidence for alteration penetrating the crystal in an irregular 'watermark' type texture from the crystal margin. Those zones are interpreted as altered have increased Sr and K, typically from ~0.02 to ~0.09 apfu and ~0.004 to ~0.02 apfu respectively during alteration (Fig. 5). In the same traverses, Ca decreases from 0.60-0.90 to <0.40 apfu and Na decreases from 0.09-0.14 to <0.05 apfu in the bright BSE, altered zones. Structural formula recalculation of altered and unaltered samples indicates development of *A*-site vacancies during alteration, with maximum values of 0.8 vacancies per formula unit. F contents decrease slightly as a result of alteration. H_2O contents inferred from low analytical totals suggest 2-5 wt% H_2O may be incorporated during this phase of alteration.

Of all of the element exchanges during alteration, the larger cations (Sr and K) best serve as chemical indicators of alteration. In unaltered samples, Sr and K are below limits of detection, however during alteration Sr can increase to 0.9 apfu, compared to unaltered values between 0-0.05. Similarly, K can occur up to 0.03 apfu in altered samples. Following the framework of Lumpkin & Ewing (1995) for the progressive alteration of minerals within the pyrochlore group, the textural and microchemical variations associated with alteration of pyrochlores from the FDF are consistent with what those authors describe as "primary alteration" associated with high temperature juvenile

fluids. The characteristic features of this are the loss of Na and F, *A*-site cation exchange for Sr, Ca, Fe and Mn, accompanied by variable changes in REE content and moderate increases in *A*-site vacancies.

MOTZFELDT SØ FORMATION PYROCHLORES

Textural character

The MSF units (including Nepheline Syenite and Altered Nepheline Syenite, Fig. 1) are not rocks with a single characteristic mineralogy and texture, but rather are definable suites of syenitic variants. Particular attention has been paid to a ***pyrochlore microsyenite*** variant within the MSF – Nepheline syenite. This is common in the roof zone of the intrusion around location 5 (Fig. 1), where alteration is most extreme and fluorite most abundant. It occurs in inclined sheets typically 10-20 cm wide without chilled contacts, demonstrating that this magma was part of the multiple episodes that gave rise to the MSF – Altered Nepheline Syenite. It is a component of the late-magmatic repeated sheeting across the whole of Location 5 and contemporaneous with it. The pyrochlore microsyenite is widespread but laterally discontinuous; individual sheets cannot be mapped across the terrain, nor correlated between drill cores. Rather it forms a swathe of minor intrusives across the whole of Location 5. Pyrochlore microsyenite comprises euhedral pink alkali feldspar crystals that are typically 1-3 mm in length, showing coarse perthite textures with an elongate tabular habit and strong mineral alignment. The modal amount of mafic minerals in the rock is typically <10%. The primary mafic mineral, usually amphibole, is largely replaced by granular clusters of Fe-Ti oxide minerals and secondary micas.

Pyrochlore crystals are common accessory minerals in several syenite facies of the MSF, but the highest concentration is in the pyrochlore microsyenite. Pyrochlore typically occurs as fine euhedral to subhedral crystals disseminated throughout the rock or as rare pyrochlore-rich veinlets. Crystals occurring in the enriched veinlets are typically 100-300 μm, compared to an average of

281 approximately 100 μm for the disseminated pyrochlore. Pyrochlore typically constitutes <15%,
282 though in some particularly enriched samples can make up approximately 25% of the rock's
283 mineralogy.

284 In contrast to the pyrochlore of the FDF, characterised by a strong honey-yellow colour in
285 transmitted light, MSF pyrochlore shows a dark reddish-brown to opaque colour in transmitted
286 light, are often rimmed by hematite and containing inclusions of alkali feldspar, Fe-Ti oxides,
287 fluorite and REE-rich carbonates, tentatively identified as bastnäsite or synchysite. BSE imaging of
288 MSF pyrochlore reveals extremely complex internal textures (Fig. 6), with very few samples
289 showing clearly recognisable primary growth zoning. In samples which retain evidence of primary
290 zonation, this is weak with secondary features overprinting them. Alteration textures within the
291 MSF pyrochlore are more intense and pervasive than the 'irregular diffusion front' texture observed
292 in the FDF samples. MSF pyrochlore displays alteration textures resembling a 'mosaic' or 'tortoise
293 shell' pattern in BSE (Fig. 6). These textures are interpreted as intense alteration associated with
294 fluid penetration largely along microfractures. The majority of pyrochlore crystals from the MSF
295 have an intermediate to bright-BSE emission which is cut by an interconnected network of darker
296 BSE vein-like areas of alteration (Fig. 6f). It has been shown in the FDF pyrochlore that primary
297 alteration (i.e. Lumpkin & Ewing 1995) increases the overall brightness of the BSE emission of the
298 crystal and give the samples a 'washed-out' appearance. In the MSF, we suggest that diffusion-
299 controlled alteration penetrated the whole crystal during a magmatic phase of alteration, increasing
300 the overall BSE emission of the crystal and washing out any primary features. These primary
301 alteration features have been subsequently overprinted by a secondary phase of lower temperature
302 alteration which appears dominantly fracture controlled. Following the classification scheme for the
303 geochemical alteration of the pyrochlore group (Lumpkin & Ewing 1995), these textural features, in
304 addition to microtextural features observed in the host rock minerals, are characteristic of the
305 process those authors described as "secondary alteration" during interaction with lower temperature
306 fluids.

In many samples showing a network of fracture related alteration, the preservation of the microfracture itself is generally rare. Lumpkin & Ewing (1995) have shown that healing of microfractures can occur in heavily altered pyrochlore through hydration and volume expansion of the pyrochlore structure. Additionally, many pyrochlores showing strong alteration associated with annealed microfractures have strong radial fractures parallel to the crystal margins, which may result from volume expansion.

Chemical effects of alteration

We have explored the microchemical variability within crystals as a function of the textures. Representative electron probe microanalyses and structural formulae of pyrochlore from the MSF are given in Table 2. Figure 7 shows the pyrochlore samples from the MSF on the Ti-Nb-Ta ternary diagram (modified after Nickel 1992). The data plot within the pyrochlore group of Hogarth (1977) and Atencio *et al.* (2010) (Fig. 7). Despite the striking differences in texture and inferred alteration histories, the chemistry of the major *B*-site cations in the MSF and FDF pyrochlores are very similar. Pyrochlore from the MSF shows a slight depletion of Nb in preference for Ti. Pyrochlore from one sample (GJM06-64) shows both secondary alteration and areas which retain earlier features. Regardless of the alteration history (magmatic, primary or secondary alteration), there is no significant change in the *B*-site chemistry (Nb, Ta and Ti) of the Motzfeldt pyrochlores. We infer that *B*-site compositional variation in pyrochlore represents an inherent magmatic feature rather than a product of alteration. None of the minor *A*-site cations exceed 20 % of the *A*-site total, with the exception of Pb which is found in two samples between 7-22 wt%. Although alteration has little influence on the B-site, chemical exchange in the cubic *A*-site is more pronounced. During primary alteration, the FDF pyrochlores show *A*-site exchange of K, Sr, Na and Ca for Fe, Mn, REEs and vacancies. Alteration within the MSF is characterised by similar trends though the more pervasive nature of the alteration produced a higher degree of exchange in the *A*-site.

Chemical effects of secondary alteration change the bulk crystal chemistry considerably; this is particularly well recorded in several pyrochlores from sample GJM06-64. Primary altered areas of pyrochlore from this sample contain significantly higher amounts of Na, Ca and F compared to areas which have experienced a secondary phase of alteration. Typical ranges for Na in primary altered areas are 0.003 to 0.590 apfu. Ca ranges from 0.179 to 0.973 apfu and F typically ranges from 0.01 to 0.89 apfu. In contrast, secondary altered areas are characterised by variable addition or removal of Ca and Na, and F fall below limits of detection. Typical compositions in these areas are 0.000 to 0.297 for Na and 0.516 to 0.952 for Ca.

Sample GJM06-64 in Figure 8 shows monovalent (A^{+}) cations (principally Na) are preferentially removed until all monovalent cations are below the limits of detection. Correspondingly, the composition moves towards the 'A-site vacancies' apex of the diagram, as divalent (A^{2+}) cations (largely Ca) are removed. This trend suggests that lower valence cations are removed preferentially at a faster rate than higher valance ones. For all other samples from the MSF, pyrochlore crystals show compositions plotting close or along the A^{2+} - *A*-site vacancies face of the diagram, suggesting effectively complete removal of Na.

Secondary alteration results in variable increases in the *A*-site cations Fe, Mn and Pb. Typical increases in these elements through alteration are 0.025 to 0.400 apfu for Fe and 0.040 to 0.140 apfu for Mn. Increases in Pb are extremely variable and highly localised, with increases up to 0.450 apfu occurring in some areas. The localised nature of such high Pb content raises some uncertainty on its structural incorporation as the high content may represent mixed analyses of microcrystalline Pb-rich inclusions, which have not been identified. Inclusions of microcrystalline galena in pyrochlores from laterite deposits have been reported by Lumpkin & Ewing (1986). Additionally such high levels of Pb incorporation would require a large increase in site vacancies to accommodate the large Pb cation. However, structural formula recalculations for Pb-rich pyrochlores in the MSF only show an increase in A-site vacancies up to 0.2 vacancies per formula unit. We suspect that the high lead content represents mixed analyses of microcrystalline Pb-bearing mineral phases hosted within the

pyrochlore, rather than localised lead enrichment in the actual pyrochlore structure. This is further supported by the fact that the occurrence of Pb to these levels is only found within two crystals from the whole dataset. As in the FDF, MSF pyrochlores are strongly enriched in the light lanthanides with La and Ce accounting for 70-85% of total REE.

U and Th contents remain relatively constant in all samples, regardless of the alteration. This suggests that any chemical variations reflect changes in the primary composition of the crystal, which are now masked by the younger pervasive alteration, rather than products of the alteration itself. Data from highly altered pyrochlores show similar compositions to the secondary altered zones observed in GJM06-64 suggesting similar trends of alteration from a similar start composition.

DISCUSSION

Genesis and conditions of alteration in the Flinks Dal Formation

The majority of the pyrochlore in the FDF syenites is euhedral, consistent with growth directly from the magma. The magmatic growth gave rise to simple oscillatory zoning patterns grading to more complex sector zoning in crystals from the FDF. In contrast, the microfracturing, radiation damage and intense compositional changes in the MSF indicate that pyrochlore group minerals from Motzfeldt also encode textural and chemical information relating to a complex magmatic history followed by multiple phases of alteration during the sub-solidus. Spatial and temporal variations in the hydrothermal activity of the centre allows the progressive alteration of pyrochlore group minerals to be studied and has provided information on the contrasting sub-solidus histories found in the mineralised units of the MSF and the less altered syenites of the FDF.

Pyrochlores from the FDF preserve oscillatory and sector zoning. In addition, from core to rim, FDF pyrochlores show a steady depletion of Ta and constant Nb content. Dark BSE zones show relative enrichment of Na, F and varied enrichment of Ca. U and Ti are notably depleted in the

darker BSE zones and show a general depletion from core-to-rim. The gradual replacement of one element for another during crystal growth can be explained by magmatic Rayleigh fractionation where one element (enriched in the core) has a greater affinity for the crystal structure than the second (enriched in the rim). Several models have been developed to explain the short period fluctuations in chemical composition that give rise to oscillatory zoning and are reviewed by Pearce (1994) and Shore & Fowler (1996). Hogarth *et al.* (2000) suggest the origin of oscillatory zoning and regular cyclic fluctuations in the composition of pyrochlore group minerals can be explained by a melt which becomes supersaturated in e.g. Nb, Ta and U rapidly precipitating these elements onto the surface of the pyrochlore and thereby reducing the concentrations around the crystal back below the saturation point. Further crystallisation increases the concentration of these elements in the melt and the process repeats. Hence oscillatory zoning does not necessarily reflect crystal growth in a dynamically changing environment. The planar nature of layer precipitation means that crystals maintain a euhedral faceted morphology throughout their growth history.

In a number of FDF pyrochlores sector zoning is also observed. Sector zoning is where precipitation onto one set of crystal faces is chemically distinct to others. It indicates anisotropy in the partitioning of particular elements on particular crystal faces. Hodgson & Le Bas (1992) examined sector-zoned pyrochlores from carbonatites on the Cape Verde Islands and suggested magma mixing to be the principal control, rather than the disequilibrium feedback model, suggesting convection and liquid mobility of the low viscosity melt would greatly inhibit the diffusion feedback mechanism. The presence of both sector and oscillatory zonation in the FDF pyrochlore minerals makes it difficult to model pyrochlore growth exclusively by one or the other of these models and is a problem raised by Hogarth *et al.* (2000). It may be that such variations in zonation are highly localised phenomena, attributed to small scale convection and mingling of comparable melts (similar P, T and *X*). Alternatively, there may be more than one generation of pyrochlore, of similar age, introduced to each other during magmatic mixing and mingling of smaller batch melts.

In addition to magmatic compositional variations, chemical changes associated with alteration are also observed in the FDF pyrochlore population. Crystals show irregular fronts of diffusive alteration cross-cutting primary growth zones. Alteration gives the crystal a 'washed-out' BSE image and is characterised by a loss of Na, Ca and F, variable increases in Sr and K and generation of *A*-site vacancies. Intra-crystalline diffusion controlled alteration has been identified in a number of studies (e.g. Chakhmouradian & Mitchell 1999, 2002; Chakoumakos & Lumpkin 1990) and has been studied in detail by Lumpkin (1989) and Lumpkin & Ewing (1992, 1995 and 1996). Lumpkin & Ewing (1995) suggest primary alteration of pyrochlore sub-group minerals, hosted within evolved high-level alkaline complexes (alkaline pegmatites, nepheline syenites and carbonatites), occur at relatively high temperatures. Chemical exchange between pyrochlore crystals and residual fluids suggest conditions of relatively high pH with high Na and Ca activity and elevated Sr activity. Because of the low degree of alteration observed in the pyrochlore crystals, hydrothermal activity in the FDF was relatively restricted compared to the more heavily altered units of the MSF. Bradshaw (1988) demonstrated that the FDF, although enriched in F, Cl and C (like many Gardar magmas), is relatively anhydrous. The elevated halogen and CO_2 content would have extended the crystallisation interval of the FDF, however hydration of primary mineral phases was relatively low due to the low water content. Therefore the diffuse alteration observed in the FDF pyrochlores is consistent with derivation from a juvenile fluid exsolved from the melt during the final stages of crystallisation, with little contribution from externally derived fluids.

Conditions of alteration in the Motzfeldt Sø Formation

Pyrochlore from the MSF shows textural and chemical features distinctive of intense and pervasive sub-solidus alteration. We infer that the alteration encoded in MSF pyrochlore was generated during multiple phases of alteration, spanning a range of thermal and chemical conditions. From observations made from FDF pyrochlore, which are thought to have crystallised from a relatively anhydrous melt, we infer that pyrochlore group minerals from the MSF experienced an extended sub-solidus history developed under a more complex hydrothermal regime, unique to the MSF,

where volatile-rich magmatically-derived fluids evolved through interaction with externally derived fluids.

The MSF is recognised as one of the first intrusive phases of the Motzfeldt centre (Emeleus & Harry 1970), emplaced into the Majût and Massartût members of the lower Eriksfjord formation (Larsen & Tukiainen 1985). Those units of the Eriksfjord comprise typically siliciclastic sediments and vesicular basalts. The FDF was emplaced later at a higher structural level into the Ilímaussaq member of the Eriksfjord Formation, comprising trachyte and phonolite (Poulsen 1964). Bradshaw (1988) suggested that the Majût and Massartût members, into which the MSF was emplaced, contained a higher proportion of formation water than the overlying Ilímaussaq member and were more permeable and susceptible to groundwater circulation. From this observation it is suggested that the interaction of juvenile fluids with thermally convected groundwater reduced the pH of the hydrothermal fluid, in the outer and upper units of the MSF, increasing the activity of Fe, Mn and REEs and promoted a secondary pervasive phase of alteration. Similar systems have been described by Andersen (1984, 1986, 1987) for the Fen carbonatite massif in Norway and by Flohr (1994) for the Magnet Cove alkaline complex in Arkansas, USA. The alteration observed in the pyrochlores from the MSF is consistent with the petrogenetic model of Bradshaw (1988) and shows many similarities to the models of Andersen (1984, 1986 and 1987) and Flohr (1994), suggesting fluid evolution leads from dominantly juvenile during the immediately post-magmatic stage, during which primary diffusive alteration occurs, to dominantly groundwater-derived aqueous fluids during lower temperature post-magmatic re-equilibration. This is supported by the fluid inclusion investigations of Schönenberger & Markl (2008), which suggests fluid contributions from both juvenile and meteoric sources. In the FDF, however, only the primary phase of alteration generated through interaction with juvenile fluids is observed. Because the FDF is completely enclosed within the MSF this would have considerably reduced the circulation of groundwaters, inhibiting the secondary lower temperature phase of alteration generated through groundwater interaction.

457 At Motzfeldt, McCreath *et al.* (2012) showed that the timing of the hydrothermal alteration
458 immediately followed magmatism. Radiation damage from U and Th in pyrochlore causes them
459 become progressively more amorphous with time. In the present study, the alteration took place
460 immediately after magmatism when the pyrochlores were predominantly crystalline. It may be that
461 had the same alteration taken place significantly later, when the pyrochlores were more amorphous,
462 different textures and geochemistry may have resulted.

463 ## CONCLUSIONS

464 Pyrochlore group minerals from the Motzfeldt centre show striking differences in texture and
465 microchemistry depending on the formation within which they are located. Samples from the Flinks
466 Dal Formation (FDF) preserve magmatic compositional zoning and are overprinted by diffuse areas
467 of alteration. In pyrochlore from the MSF, primary features are wholly overprinted by pervasive
468 alteration, characterising a different subsolidus history to the pyrochlores of the FDF. Pyrochlore
469 crystals therefore serve as a useful indicator of the different geochemical conditions which the rocks
470 of MSF and FDF experienced during the subsolidus evolution of the centre. Pyrochlore group
471 minerals from the FDF display concentric growth zones and sector zoning characterising
472 compositional fluctuation in the magma chamber during the evolution of the host melt. Although
473 most pyrochlore crystals from the FDF contain areas that are pristine, a number of samples have
474 undergone subsolidus alteration, characterised by removal of Na & Ca and variable addition of Sr &
475 K. Textures associated with this phase of alteration form a clear diffusive front penetrating into the
476 crystal. The textural and chemical character of alteration in the FDF is consistent with a relatively
477 high temperature phase of alteration associated with the final stages of crystallisation. In the MSF
478 the textural character of alteration is intense and pervasive, penetrating pyrochlore through a
479 network of microfractures. During this phase of alteration, pyrochlores are leached of cations and,
480 based on the low totals observed by EPMA, significantly hydrated in the presence of a lower
481 temperature evolved hydrothermal fluid. The alteration encoded in the pyrochlores of the present

482 study therefore reflects the different hydrothermal conditions the MSF and FDF experienced during
483 the subsolidus and shows how evolution of fluids within one intrusive unit can vary both spatially
484 and temporally.

485 The fact that the MSF is particularly rich in Ta, Nb and REE, and that the MSF has been subjected
486 to multiple phases of hydrothermal alteration, may superficially suggest that the hydrothermal
487 alteration is linked to an enrichment process for the elements of commercial interest. However our
488 data demonstrate that the high field strength *B*-site elements such as Nb, Ta are largely unchanged
489 during the hydrothermal alteration of the pyrochlore. Thus the commercially interesting amounts of
490 these elements were present in pyrochlore at the magmatic stage. The Ta and Nb contents of the
491 pyrochlore are increased during alteration, but this is because of exchange of relative light elements
492 for heavier elements onto A-sites and the formation of A-site vacancies, making the same number
493 of Ta and Nb atoms constitute a large % of the whole. Hydrothermal alteration has had no
494 discernable influence on the tonnage of these elements at Motzfeldt. However the alteration may
495 influence the ease of extraction of high field strength elements from the pyrochlore. Hydrothermally
496 altered pyrochlore has substantial A-site vacancies which may influence nanoporosity and reactivity
497 to acids; magmatic and hydrothermally altered pyrochlore may display substantially different
498 digestion rates and single crystals comprising a mosaic of magmatic and hydrothermally altered
499 pyrochlore may have e.g. soluble rims and refractory cores. Radioactive elements, notably U, create
500 radiation damage and metamict (partly amorphous) structural domains. Although we show all the
501 pyrochlore of the present study is grossly stoichiometric, the constraints on stoichiometry that can
502 be applied to pyrochlore are far laxer than for most mineral systems. The pyrochlores of the present
503 study, particularly hydrothermally altered ones, may contain discreet nanoparticulate secondary
504 phases or partly amorphous nanodomains. Such complexity could have substantial effects on the
505 possible yield.

506 ## ACKNOWLEDGEMENTS

Work for the present study was carried out during tenure of a postgraduate studentship funded by Angus and Ross plc. Johannes Schönenberger (University of Tübingen, Germany) is gratefully thanked for samples and for assistance in the field. The constructive and thoughtful reviews of Greg Lumpkin and Fabio Bellatreccia improved the manuscript greatly.

REFERENCES CITED

Allart, J.H. (1976) Ketilidian mobile belt in South Greenland. Pp. 121-151 in: Geology of Greenland (Escher, A and Watt, W.S. editors). Geological Survey of Greenland, Copenhagen, Denmark.

Andersen, T. (1984) Secondary processes in carbonatites: Petrology of "Rødberg" (hematite-calcite-dolomite carbonatite) in the Fen central complex, Telemark (South Norway). Lithos, 17, 227-245.

Andersen, T. (1986) Magmatic fluids in the Fen carbonatite complex, S.E. Norway. Contributions to Mineralogy and Petrology, 93, 491-503.

Andersen, T. (1987) A model for the evolution of hematite carbonatite, based on whole-rock major and trace element data from the Fen complex, Southeast Norway. Applied Geochemistry, 2, 163-180.

Armour-Brown, A. (2001) Tantalum exploration: Review of Previous exploration, results of beneficiation studies and recommendations for future work, Angus & Ross plc, report 1.

Armour-Brown, A., Tukiainen, T., Wallin, B., Bradshaw, C. and Emeleus, C.H. (1983) Uranium exploration in South Greenland. Rapport Grønlands Geologiske Undersøgelse, 115, 68-75.

Atencio, D., Andrade, M.B., Christy, A.G., Gieré, R., and Kartashov, P.M., (2010) The Pyrochlore Supergroup of Minerals: Nomenclature. The Canadian Mineralogist, 48, 673-698.

Blaxland, A.B., van Breemen, O., Emeleus, C.H., and Anderson, J.G. (1978) Age and origin of

529 major syenite centers in Gardar Province of South Greenland - Rb-Sr studies. Geological Society of
530 America Bulletin, 89, 231-244.

531 Bonazzi, P., Bindi, L., Zoppa, M., Capitain, G. and Olmi, F. (2006) Single-crystal diffraction and
532 transmission electron microscopy studies of "silicified" pyrochlore from Narssarssuk, Julianehåb
533 district, Greenland. American Mineralogist, 91, 794-801.

534 Bradshaw, C. (1985) The Alkaline rocks of the Motzfeldt Centre: Progress report on the 1984 field
535 season. Rapport Grønlands Geologiske Undersøgelse, 125, 62-64.

536 Bradshaw, C. (1988) A petrographic, structural and geochemical study of the alkaline igneous rocks
537 of the Motzfeldt centre, South Greenland. Unpublished PhD thesis, University of Durham, UK.

538 Chakhmouradian, A.R. and Mitchell, R.H. (1999) Primary, agpaitic and deuteric stages in the
539 evolution of accessory Sr, REE, Ba and Nb-mineralisation in nepheline-syenite pegmatites at
540 Pegmatite peak, Bearpaw mountains, Montana. Mineralogy and Petrology, 67, 85-110.

541 Chakhmouradian, A.R. and Mitchell, R.H. (2002) New data on pyrochlore- and perovskite-group
542 minerals from the Lovozero alkaline complex, Russia. European Journal of Mineralogy, 14, 821-
543 836.

544 Chakoumakos, B.C. (1984) Systematics of the pyrochlore structure type, ideal $A_2B_2X_6Y$. Journal of
545 Solid State Chemistry, 53, 120-129.

546 Chakoumakos, B.C. and Lumpkin, G.R. (1990) Pressure-temperature constraints on the
547 crystallisation of the Harding pegmatite, Taos Country, New Mexico. Canadian Mineralogist, 28,
548 287-98.

549 Edge, R.A., and Taylor, H.F.W. (1969) Crystal structure of thaumasite, a mineral containing
550 $[Si(OH)_6]^{2-}$ groups. Nature, 224, 364

551 Emeleus, C.H. and Harry, W.T. (1970) The Igaliko nepheline syentie complex. General description.
552 Grønlands Geologiske Undersøgelse Bulletin, 85, 116.

553 Finger, L.W. and Hazen, R. (1991) Crystal chemistry of six-coordinated silicon: A key to
554 understanding the earth's deep interior. Acta Crystallographica, 47, 561-580.

555 Flohr, M.J.K. (1994) Titanium, vanadium and niobium mineralisation and alkali metasomatism
556 from the Magnet Cove Complex, Arkansas. Economic Geology, 89, 105-130.

557 Hodgson, N.A. and Le Bas, M.J. (1992) The chemistry and cryptic zonation of pyrochlore from San
558 Vicente, Cape Verde Islands. Mineralogical Magazine, 56, 201-214.

559 Hogarth, D.D. (1977) Classification and nomenclature of the pyrochlore group. American
560 Mineralogist, 35, 403-410.

561 Hogarth, D.D., Williams, C.T. and Jones, P. (2000) Primary zoning in pyrochlore group minerals
562 from carbonatites. Mineralogical Magazine, 64, 683-697.

563 Johan, V. and Johan, Z. (1994) Accessory minerals of the Cinovec (Zinnwald) granite cupola,
564 Czech Republic Part 1: Nb-, Ta-, and Ti-bearing oxides. Mineralogy and Petrology, 51, 323-343.

565 Jones, A.P. (1980) The petrology and structure of the Motzfeldt centre, Igaliko, South Greenland.
566 Unpublished PhD thesis. University of Durham, UK.

567 Larsen, L.M., and Tukiainen, T. (1985) New observations on the easternmost extension of the
568 Gardar supracrustals (Eriksfjord Formation), South Greenland. Rapport Grønlands Geologiske
569 Undersøgelse, 125, 64-66.

570 Luca, V., Griffith, C., Blackford, M. and Hanna, J. (2005) Structural and ion exchange properties of
571 nanocrystalline Si-doped antimony pyrochlore. Journal of Materials Chemistry, 15, 564-572.

572 Lumpkin, G. (1989) Alpha-decay damage, geochemical alteration and crystal chemistry of

pyrochlore group minerals. Unpublished PhD thesis. University of New Mexico, USA.

Lumpkin, G.R. and Ewing, R.C. (1988) Alpha-Decay Damage in Minerals of the Pyrochlore Group. Physics and Chemistry of Minerals, 16, 2-20.

Lumpkin, G.R. and Ewing, R.C. (1992) Geochemical alteration of pyrochlore group minerals: Microlite subgroup. American Mineralogist, 77, 179-188.

Lumpkin, G.R. and Ewing, R.C. (1995) Geochemical alteration of pyrochlore group minerals: Pyrochlore subgroup. American Mineralogist, 80, 732-743.

Lumpkin, G.R. and Ewing, R.C. (1996) Geochemical alteration of pyrochlore group minerals: Betafite subgroup. American Mineralogist, 81, 1237-1248.

McCreath, J.A. (2009) Petrology and petrogenesis of the Motzfeldt Ta-mineralisation, Gardar Province, South Greenland. Unpublished PhD thesis, University of St Andrews, UK.

McCreath, J.A., Finch, A.A., Simonsen, S.L., Donaldson, C.H. and Armour-Brown, A. (2012) Independent ages of magmatic and hydrothermal activity in alkaline igneous rocks: The Motzfeldt Centre, Gardar Province, South Greenland. Contributions to Mineralogy and Petrology, 163, 967-982.

Nickel, E. (1992) Solid solutions in mineral nomenclature. Canadian Mineralogist, 30, 231-234.

Pearce, T.H. (1994) Recent work on oscillatory zoning in plagioclase. Pp. 313-349 in: Feldspars and their Reactions (I. Parsons editor). Kluwer Academic, Dordrecht.

Poulsen, V. (1964) The sandstones of the Precambrian Eriksfjord Formation in South Greenland. Rapport Grønlands Geologiske Undersøgelse, 2, 16.

Ross, N., Shu, J., Hazen, R., and Gasparik, T. (1990) High-pressure crystal chemistry of stishovite. American Mineralogist, 75, 739-747.

595 Schonenberger J and Markl G (2008) The magmatic and fluid evolution of the Motzfeldt intrusion
596 in South Greenland: Insights into the formation of agpaitic and miaskitic rocks. Journal of
597 Petrology, 49, 1549-1577.

598 Shore, M. and Fowler, A.D. (1996) Oscillatory zoning in minerals: A common phenomenon.
599 Canadian Mineralogist, 34, 1111-1126.

600 Thomassen, B. (1988) The Motzfeldt 87 Project, Final Report. Open file Series 88/1, Grønlands
601 Geologiske Undersøgelse.

602 Tukiainen, T. (1988) Niobium-tantalum mineralisation in the Motzfeldt centre of the Igaliko
603 nepheline syenite complex, South Greenland. Pp. 230-46 in. Mineral deposits within the European
604 Community (J. Boissonnas, and P. Omenetto, editors). Springer-Verlag, Berlin Heidelberg.

605 Tukiainen, T., Bradshaw, C. and Emeleus, C.H. (1984) Geological and radiometric mapping of the
606 Motzfeldt centre of the Igaliko Complex, South Greenland. Rapport Grønlands Geologiske
607 Undersøgelse, 102, 78-83.

608 Upton, B.G.J. and Emeleus, C.H. (1987) Mid-Proterozoic alkaline magmatism in Southern
609 Greenland. Pp. 449-471 in: Alkaline Igneous Rocks (J.G. Fitton, and B.G.J. Upton editors).
610 Geological Society of London, Special Publication 30, Blackwells, Oxford, UK.

611 Upton, B.G.J., Emeleus, C.H., Heaman, L.M., Goodenough, K.M. and Finch, A.A. (2003)
612 Magmatism of the Mid-Proterozoic Gardar Province, South Greenland: Chronology, petrogenesis
613 and geological setting. Lithos, 68, 43-65.

614 Voloshin, A., Pakhomovskiy, Y., Nadezhina, T., Bakhchisaraitsev, A., and Kobyashev, Y. (1989)
615 Strontiopyrochlore: Composition and structure. Trudy Mineralogicheskogo Muzeya SSSR, 36, 12-
616 24 (In Russian).

617

FIGURE CAPTIONS

FIG. 1. Geological map of Motzfeldt alkaline centre (after Bradshaw 1988; Jones 1980; Tukiainen et al. 1984). Numbers in circles refer to locations identified by Angus & Ross plc during their exploration of the area.

FIG. 2: Back-Scattered Electron (BSE) images of pyrochlore crystals from the Flinks Dal formation. (a), (b) and (d) Oscillatory zoned pyrochlore crystals. (c) Sector-zoned pyrochlore crystal. (e) and (f) oscillatory and sector-zoned pyrochlore crystals showing a dark backscatter emission band (black arrow) interpreted as a diffusive alteration front and primary altered areas (light BSE washed-out areas).

FIG. 3. B-site element chemistry of pyrochlore group minerals from the Flinks Dal formation (samples JS53, JS55 and JS66), projected onto the Nb-Ta-Ti ternary diagram. The analytical precision in EPMA corresponds to uncertainties equivalent to the size of the symbols.

FIG. 4. Distribution of Na, Ca, Mn, U, Nb, Ta and Ti from core to rim across oscillatory and sector zoned pyrochlore crystals from the Flinks Dal formation. Na, Ca and Nb are shown as cation/10, apart from samples JS53-2 and JS53-5, which are shown as true values. Distribution profiles have been scaled and are not true traverse distances. Dark grey bands correspond to dark backscatter emission zones and light grey to bright back scatter emission zones. The analytical precision in EPMA corresponds to uncertainties equivalent to the size of the symbols.

FIG. 5. Variation diagrams (apfu) for large A-site cations (Sr, K, Na and Ca) vs. A-site vacancies for unaltered and altered pyrochlore areas. Arrows show alteration trends. Note that the decreases in Ca in high-BSE zones is a primary compositional feature and not a product of alteration. Shaded area shows field of entire data set of unaltered Flinks Dal formation pyrochlore samples. The analytical precision in EPMA corresponds to uncertainties equivalent to the size of the symbols.

641 FIG. 6. BSE images of pyrochlore crystals from the Motzfeldt Sø formation. (a) and (b) Pyrochlores
642 retaining weak primary zones overprinted by mosaic of alteration. (c), (d) and (e) Heavily altered
643 pyrochlore crystals with intense network of microfractures penetrating the whole crystal (dark grey
644 BSE emission) (f) close up of pyrochlore in (e) showing the network of microfractures and
645 associated dark BSE alteration.

646 FIG. 7. B-site element chemistry of pyrochlore group minerals from the Motzfeldt Sø Formation
647 (samples GJM06-21, GJM0-24, GJM06-44 and GJM06-64), projected onto the Nb-Ta-Ti ternary
648 diagram. Shaded field shows the field for unaltered pyrochlores from the Flinks Dal Formation. The
649 analytical precision in EPMA corresponds to uncertainties equivalent to the size of the symbols.

650 FIG. 8. Ternary variation diagram for divalent A-site cations (Ca, Fe, Mn and Sr), Monovalent A-
651 site cations (Na) and A-site vacancies in samples from the MSF. Sample GJM06-64 shows analyses
652 from areas only altered during a primary high temperature phase of alteration in addition to analyses
653 of secondary altered areas. All other samples are from altered areas. The analytical precision in
654 EPMA corresponds to uncertainties equivalent to the size of the symbols.
655

656 TABLE 1. Representative EPMA of pyrochlore from the Flinks Dal formation.

Wt.%	**Light BSE magmatic zones**			**Dark BSE magmatic zones**			**Altered zones**		
Na_2O	5.87	7.41	5.76	5.71	6.60	4.10	0.25	0.37	0.74
CaO	16.85	13.95	9.70	14.64	16.19	12.50	4.65	6.73	9.58
K_2O	n.d.	n.d.	n.d.	n.d.	n.d.	n.d.	0.37	0.32	0.3
MnO	0.62	0.52	0.52	0.03	0.04	1.10	0.4	0.37	0.3
SrO	0.27	0.42	1.44	0.23	0.25	0.67	2.48	2.34	1.35
PbO	0.04	n.d.	0.78	n.d.	n.d.	0.24	0.77	n.d.	0.05
ThO_2	0.21	0.20	0.19	0.27	0.67	0.10	n.d.	n.d.	n.d.
UO_2	2.66	2.53	4.31	1.22	1.59	3.03	2.94	2.17	0.79
La_2O_3	0.65	0.55	0.24	0.36	0.30	0.55	0.47	0.5	0.56
Ce_2O_3	1.72	1.32	1.28	1.24	0.94	1.59	0.63	0.89	0.98
Pr_2O_3	0.14	0.24	0.07	n.d.	0.13	0.14	n.d.	n.d.	n.d.
Nd_2O_3	0.45	0.24	0.48	0.42	0.43	0.73	0.39	0.43	0.36
Sm_2O_3	0.10	0.29	0.30	0.13	0.07	0.16	n.d.	n.d.	n.d.
Gd_2O_3	0.02	0.11	n.d.	n.d.	0.16	n.d.	0.29	0.16	n.d.
Dy_2O_3	0.06	n.d.	0.30	0.22	0.12	n.d.	0.33	0.17	0.01
SiO_2	0.20	1.54	n.d.	0.25	0.10	3.37	n.d.	n.d.	n.d.
ZrO_2	0.58	0.91	1.37	2.26	0.82	0.16	1.33	2.18	2.35
Nb_2O_5	60.82	62.36	62.34	61.27	62.64	57.67	59.96	61.04	56.36
Ta_2O_5	1.34	1.53	2.63	3.27	1.57	1.02	2.81	2.71	3.97
TiO_2	4.07	3.64	4.39	3.82	3.89	5.00	4.49	4.02	3.85
FeO	0.21	0.35	1.04	0.27	0.03	2.06	0.79	0.57	1.03
F	3.00	3.93	3.59	6.16	3.60	3.02	0.8	2.44	1.02
Sum	99.87	102.03	100.73	101.77	100.14	97.23	84.15	87.41	83.60
O≡F	-1.26	-1.65	-1.51	-2.59	-1.52	-1.27	-0.34	-1.03	-0.43
Total	**98.61**	**100.37**	**99.22**	**99.18**	**98.63**	**95.96**	**83.81**	**86.38**	**83.17**
Structural Formulae (∑B-site cations = 2)									
Na	0.364	0.452	0.340	0.340	0.399	0.263	0.015	0.022	0.047
Ca	1.157	0.940	0.632	0.963	1.082	0.887	0.312	0.445	0.671
Mn	-	-	-	-	-	-	0.030	0.025	0.025
K	0.034	0.028	0.027	0.002	0.002	0.062	0.021	0.019	0.017
Sr	0.010	0.015	0.051	0.008	0.009	0.026	0.090	0.084	0.051
Pb	0.001	-	0.013	-	-	0.004	0.013	-	0.001
Th	0.003	0.003	0.003	0.004	0.010	0.001	-	-	-
U	0.038	0.035	0.058	0.017	0.022	0.045	0.041	0.030	0.011
La	0.015	0.013	0.005	0.008	0.007	0.013	0.011	0.011	0.013
Ce	0.040	0.030	0.028	0.028	0.022	0.039	0.014	0.020	0.023
Pr	0.003	0.005	0.002	-	0.003	0.003	-	-	-
Nd	0.010	0.005	0.010	0.009	0.010	0.017	0.009	0.009	0.008
Sm	0.002	0.006	0.006	0.003	0.002	0.004	-	-	-
Gd	0.001	0.002	-	-	0.003	-	0.006	0.003	-
Dy	0.001	-	0.006	0.004	0.002	-	0.007	0.003	-
Si	0.013	0.097	-	0.016	0.006	0.223	-	-	-
Fe	0.011	0.018	0.053	0.014	0.002	0.114	0.041	0.029	0.056
∑A	**1.704**	**1.651**	**1.234**	**1.415**	**1.579**	**1.703**	**0.611**	**0.702**	**0.925**
∑REE	0.073	0.062	0.058	0.052	0.049	0.077	0.047	0.048	0.046
Nb	1.762	1.774	1.715	1.701	1.766	1.727	1.700	1.702	1.665
Ta	0.023	0.026	0.043	0.055	0.027	0.018	0.048	0.045	0.071
Ti	0.196	0.172	0.201	0.176	0.182	0.249	0.212	0.187	0.189
Zr	0.018	0.028	0.041	0.068	0.025	0.005	0.041	0.066	0.075
∑B	**2.000**	**2.000**	**2.000**	**2.000**	**2.000**	**2.000**	**2.000**	**2.000**	**2.000**
F	0.496	0.620	0.602	0.984	0.584	0.509	0.170	0.480	0.213

All Fe is assumed to be Fe^{2+} and allocated to the A-site. n.d. = not detected. Samples donated by J. Schönenberger.

657

658 TABLE 2. Representative EPMA of pyrochlore from the Motzfeldt Sø formation.

Wt.%	Primary Altered Zones					Secondary Altered Zones				
Na_2O	0.17	6.00	4.69	n.d.	3.23	0.77	0.89	n.d.	0.29	1.28
CaO	4.78	10.38	9.52	6.45	10.39	9.33	10.61	7.33	9.17	12.47
MnO	n.d.	0.11	0.02	n.d.	n.d.	0.13	0.08	0.26	0.04	0.01
K_2O	2.46	0.05	0.10	1.84	0.41	0.25	0.08	n.d.	0.72	n.d.
SrO	0.58	0.08	0.04	1.00	0.10	1.12	0.09	1.23	1.15	1.59
PbO	0.07	0.23	0.49	n.d.	0.16	0.15	0.24	1.05	n.d.	0.52
ThO_2	n.d.	0.17	0.31	0.15	0.23	0.27	0.44	0.27	0.20	0.16
UO_2	3.08	3.89	3.71	3.54	3.85	4.33	3.63	2.34	4.73	2.28
La_2O_3	0.61	0.96	1.54	1.20	1.05	0.80	1.09	1.12	1.09	1.07
Ce_2O_3	1.58	2.45	2.52	2.33	2.21	2.36	2.72	n.d.	2.90	n.d.
Pr_2O_3	0.01	n.d.	0.40	0.13	0.19	0.24	0.24	n.d.	0.10	n.d.
Nd_2O_3	0.45	0.87	0.81	0.83	0.64	0.50	0.73	0.30	0.35	0.29
Sm_2O_3	n.d.	0.21	0.18	n.d.	0.16	n.d.	0.12	0.18	n.d.	n.d.
Gd_2O_3	n.d.	n.d.	n.d.	n.d.	n.d.	0.02	0.00	n.d.	n.d.	0.07
Dy_2O_3	n.d.	0.01	0.04	n.d.	0.18	0.00	0.07	0.85	0.20	1.41
SiO_2	2.67	1.52	1.33	2.55	2.41	6.57	2.81	5.49	2.79	2.89
ZrO_2	0.56	1.10	1.15	1.01	1.25	0.92	0.94	0.73	0.66	0.58
Nb_2O_5	58.24	55.70	56.07	53.61	58.41	48.90	54.31	50.33	46.09	49.28
Ta_2O_5	4.78	5.16	5.71	5.18	4.31	6.05	5.32	4.94	7.40	4.90
TiO_2	8.35	8.01	7.97	7.83	7.89	7.19	7.38	7.96	8.37	6.36
FeO	7.45	0.18	0.07	7.51	0.36	2.33	0.27	5.67	1.98	2.25
F	n.d.	n.d.	2.16	0.57	1.23	0.44	0.18	n.d.	0.32	n.d.
Sum	95.84	97.08	98.83	95.73	98.66	92.67	92.24	90.05	88.55	87.41
O≡F	0.00	0.00	0.91	0.24	0.52	0.19	0.08	0.00	0.13	0.00
Total	**95.84**	**97.08**	**97.92**	**95.49**	**98.14**	**92.48**	**92.16**	**90.05**	**88.42**	**87.41**
Structural Formulae (∑B-site cations = 2)										
Na	0.010	0.351	0.272	-	0.183	0.050	0.054	-	0.019	0.087
Ca	0.300	0.671	0.610	0.432	0.652	0.675	0.710	0.516	0.667	0.932
Mn	-	0.008	0.002	-	-	0.011	0.006	0.022	0.003	0.001
K	0.122	0.003	0.005	0.097	0.020	0.014	0.004	-	0.041	-
Sr	0.020	0.003	0.001	0.036	0.003	0.044	0.003	0.047	0.045	0.064
Pb	0.001	0.004	0.008	-	0.003	0.003	0.004	0.019	-	0.010
Th	-	0.002	0.004	0.002	0.003	0.004	0.006	0.004	0.003	0.003
U	0.040	0.052	0.049	0.049	0.050	0.065	0.050	0.034	0.071	0.035
La	0.013	0.021	0.034	0.028	0.023	0.020	0.025	0.027	0.027	0.028
Ce	0.034	0.054	0.055	0.053	0.047	0.058	0.062	-	0.072	-
Pr	0.000	-	0.009	0.003	0.004	0.006	0.005	-	0.002	-
Nd	0.009	0.019	0.017	0.019	0.013	0.012	0.016	0.007	0.008	0.007
Sm	-	0.004	0.004	-	0.003	-	0.003	0.004	-	-
Gd	-	-	-	-	-	-	-	-	-	0.002
Dy	-	-	0.001	-	0.003	-	0.001	0.018	0.004	0.032
Si	0.156	0.092	0.080	0.159	0.141	0.444	0.176	0.361	0.189	0.202
Fe	0.365	0.009	0.003	0.392	0.018	0.132	0.014	0.312	0.112	0.131
∑***A***	1.069	1.294	1.153	1.270	1.169	1.539	1.142	1.370	1.267	1.532
∑REE	0.057	0.099	0.120	0.102	0.094	0.097	0.113	0.056	0.115	0.068
Nb	1.541	1.519	1.515	1.514	1.548	1.493	1.534	1.495	1.414	1.554
Ta	0.076	0.085	0.093	0.088	0.069	0.111	0.090	0.088	0.137	0.093
Ti	0.367	0.363	0.358	0.368	0.348	0.365	0.347	0.393	0.427	0.334
Zr	0.016	0.032	0.034	0.031	0.036	0.030	0.029	0.023	0.022	0.020
∑***B***	2.000	2.000	2.000	2.000	2.000	2.000	2.000	2.000	2.000	2.000
F	-	-	0.370	0.106	0.210	0.081	0.034	-	0.064	-

All Fe is assumed to be Fe^{2+} and allocated to the A-site n.d. = not detected.

659

61° 15′N

0 km 5

N

Flinks Dal fault

Flinks Dal Fault

Motzfeldt

Qoroq

45°W

Flink's Dal Formation

- Nepheline syenite
- Porphyritic syenite
- Foyaite

Motzfeldt Sø Formation

- Nepheline syenite
- Altered nepheline syenite
- Marginal arf. syenite

Sheet Intrusives

- Peralkaline microsyenite
- Larvikite(L) Syenogabbro(S)
- Alkali syenite
- Lujavrite

Geologfjeld Formation

- Geologfjeld nepheline syenite

Country Rocks

- Eriksfjord supracrustals
- Ketilidian basement
- North Motzfeldt NM1
- North Motzfeldt NM2
- Glaciers
- Major faults
- Location Numbers

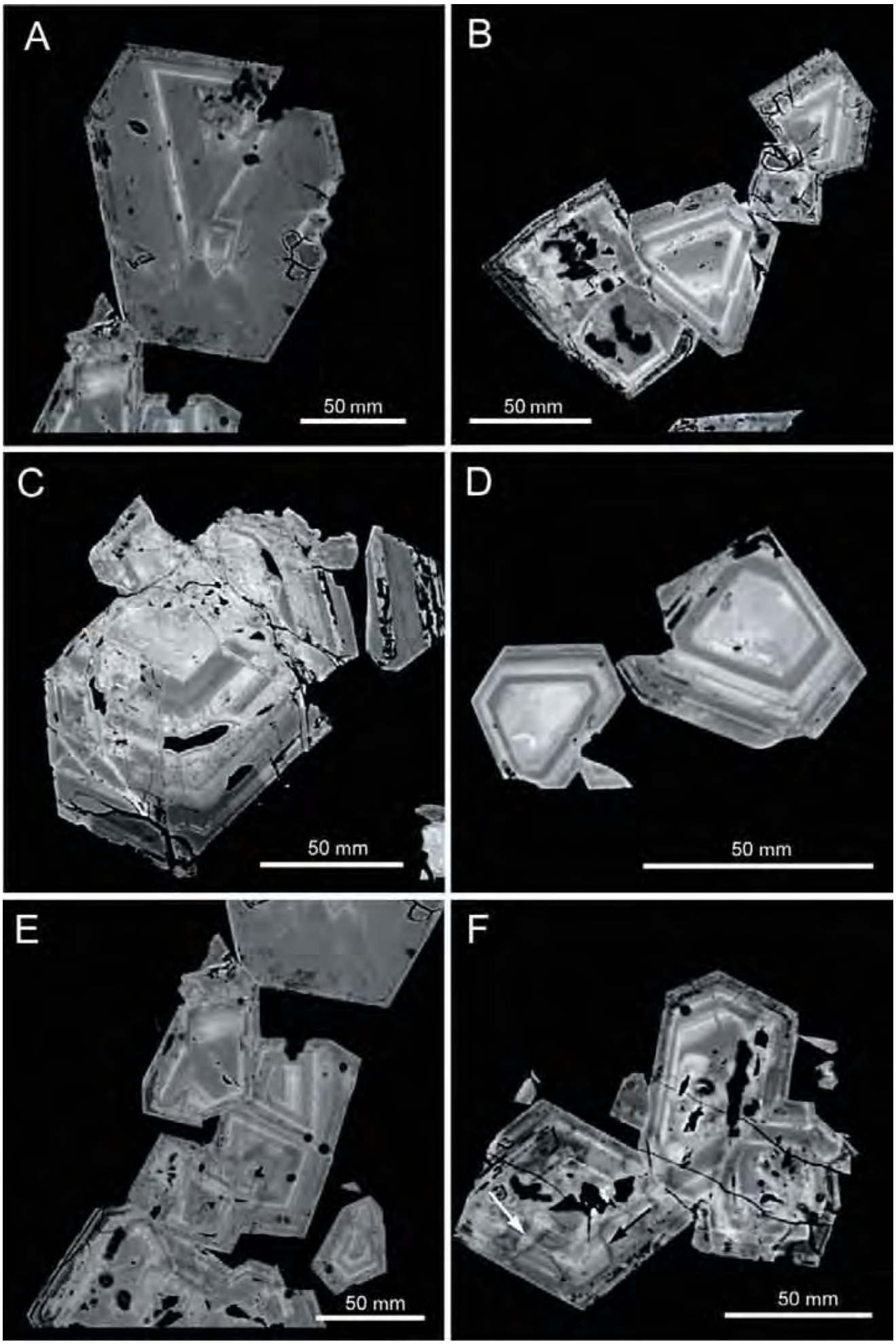
A
50 mm
B
50 mm
C
50 mm
D
50 mm
E
50 mm
F
50 mm

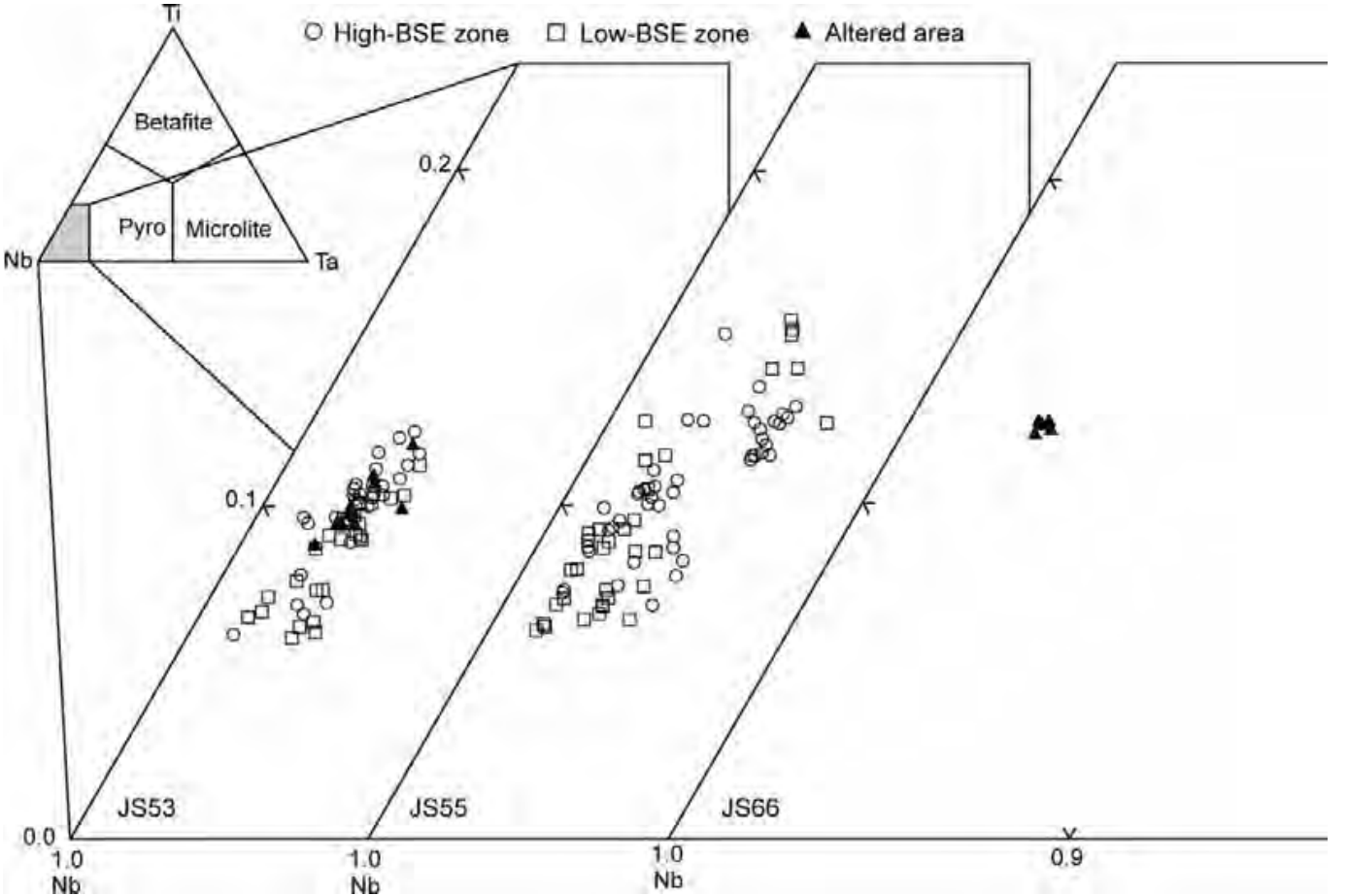
Ti
High-BSE zone
Low-BSE zone
Altered area
Betafite
Pyro
Microlite
Nb
Ta
0.2
0.1
0.0
JS53
JS55
JS66
1.0
Nb
1.0
Nb
1.0
Nb
0.9
Y

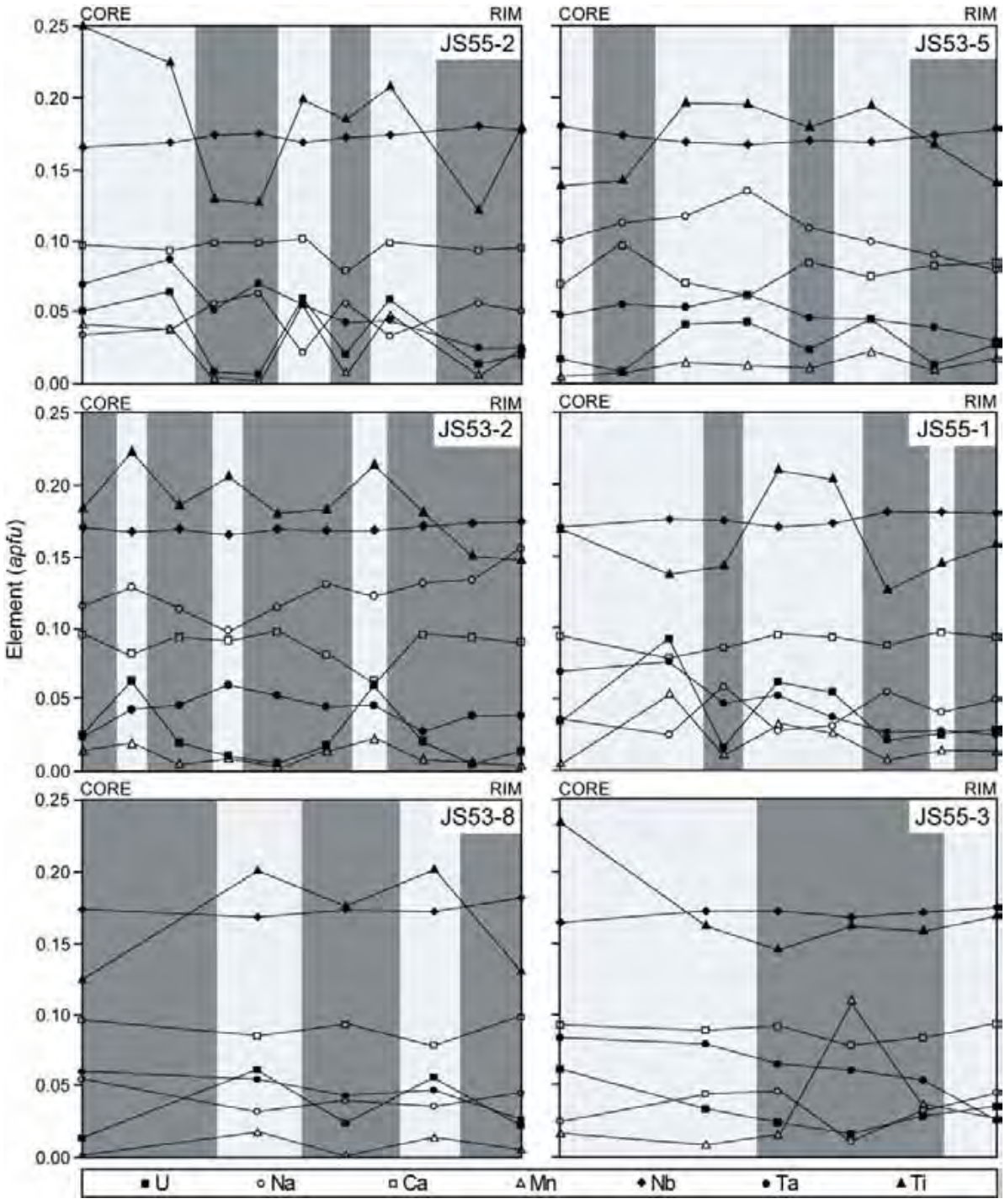
CORE
RIM
JS55-2
JS53-5
JS53-2
JS55-1
JS53-8
JS55-3
Element (apfu)
0.25
0.20
0.15
0.10
0.05
0.00
U
Na
Ca
Mn
Nb
Ta
Ti

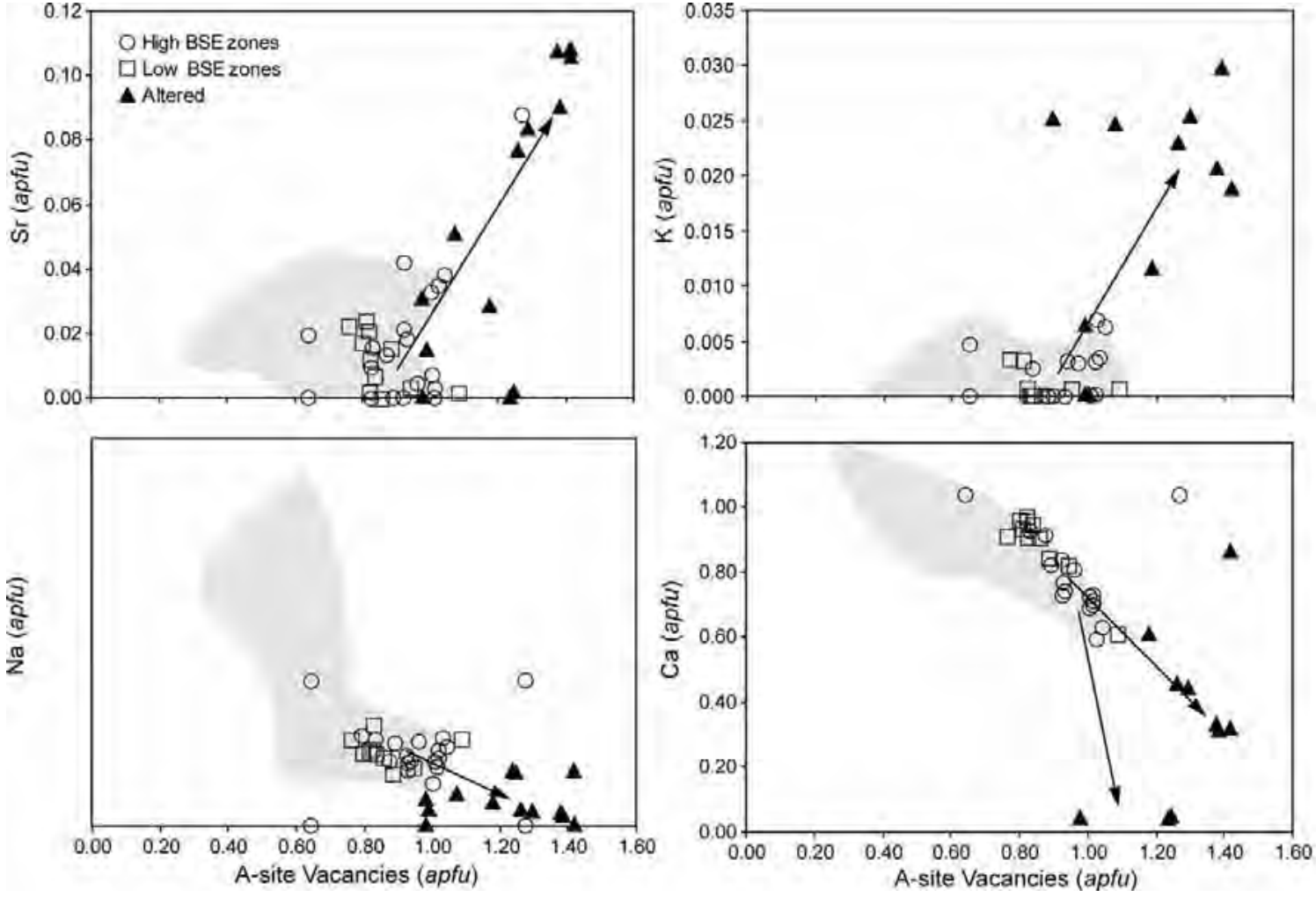
High BSE zones
Low BSE zones
Altered
Sr (apfu)
K (apfu)
Na (apfu)
Ca (apfu)
A-site Vacancies (apfu)
A-site Vacancies (apfu)

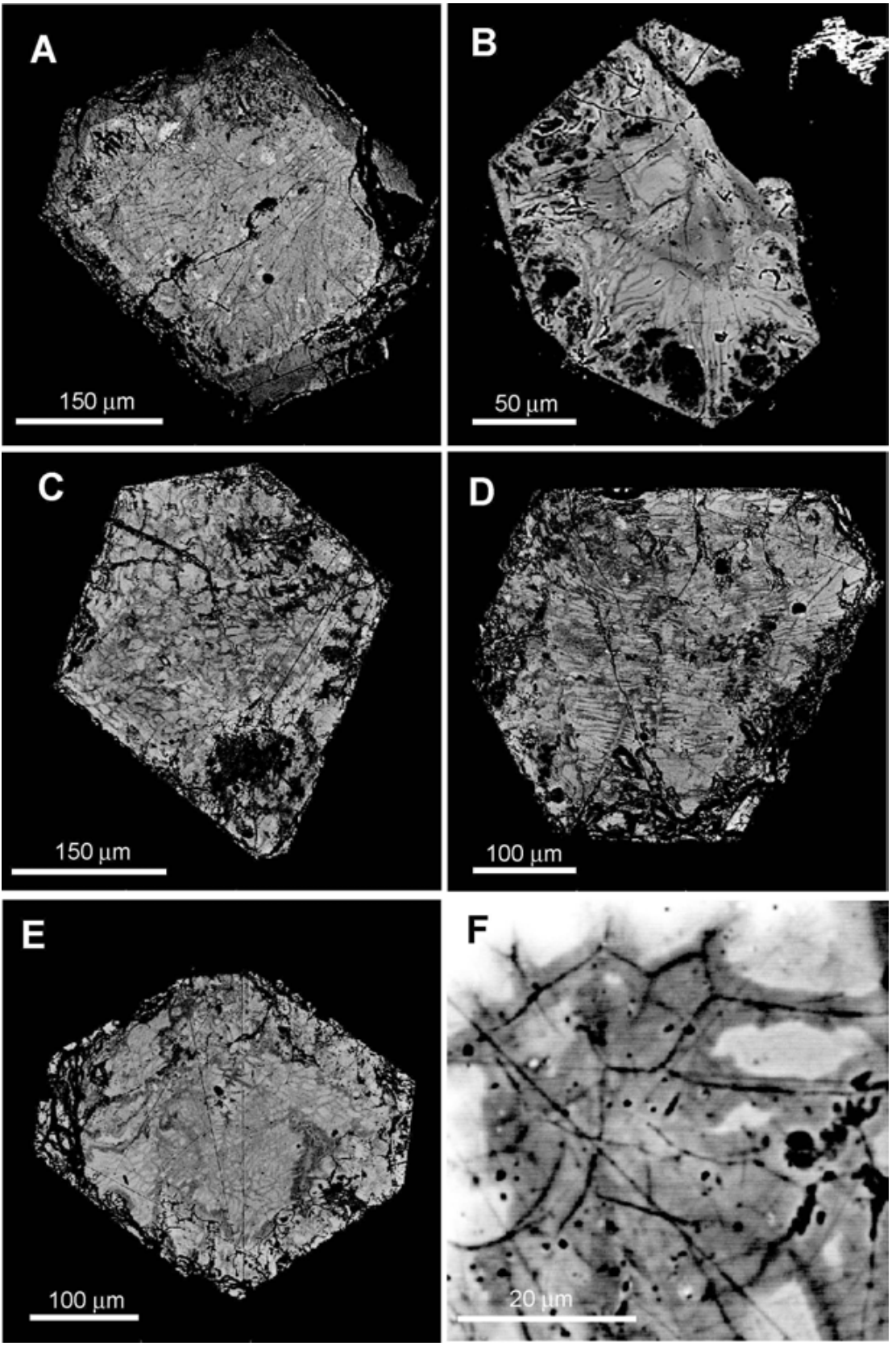
A
150 µm
B
50 µm
C
150 µm
D
100 µm
E
100 µm
F
20 µm

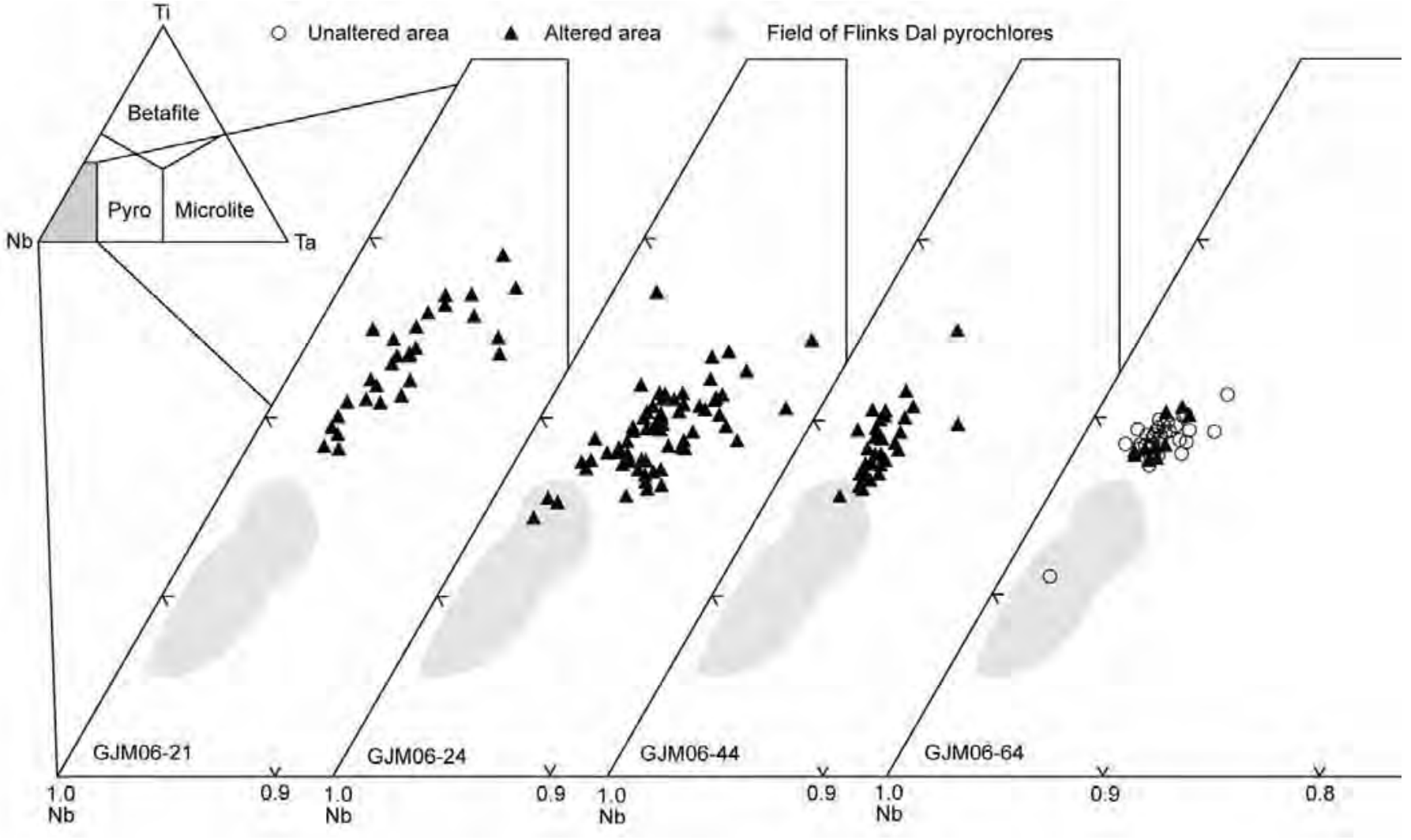
Ti
Unaltered area
Altered area
Field of Flinks Dal pyrochlores
Betafite
Pyro
Microlite
Nb
Ta
GJM06-21
GJM06-24
GJM06-44
GJM06-64
1.0
Nb
0.9
0.8

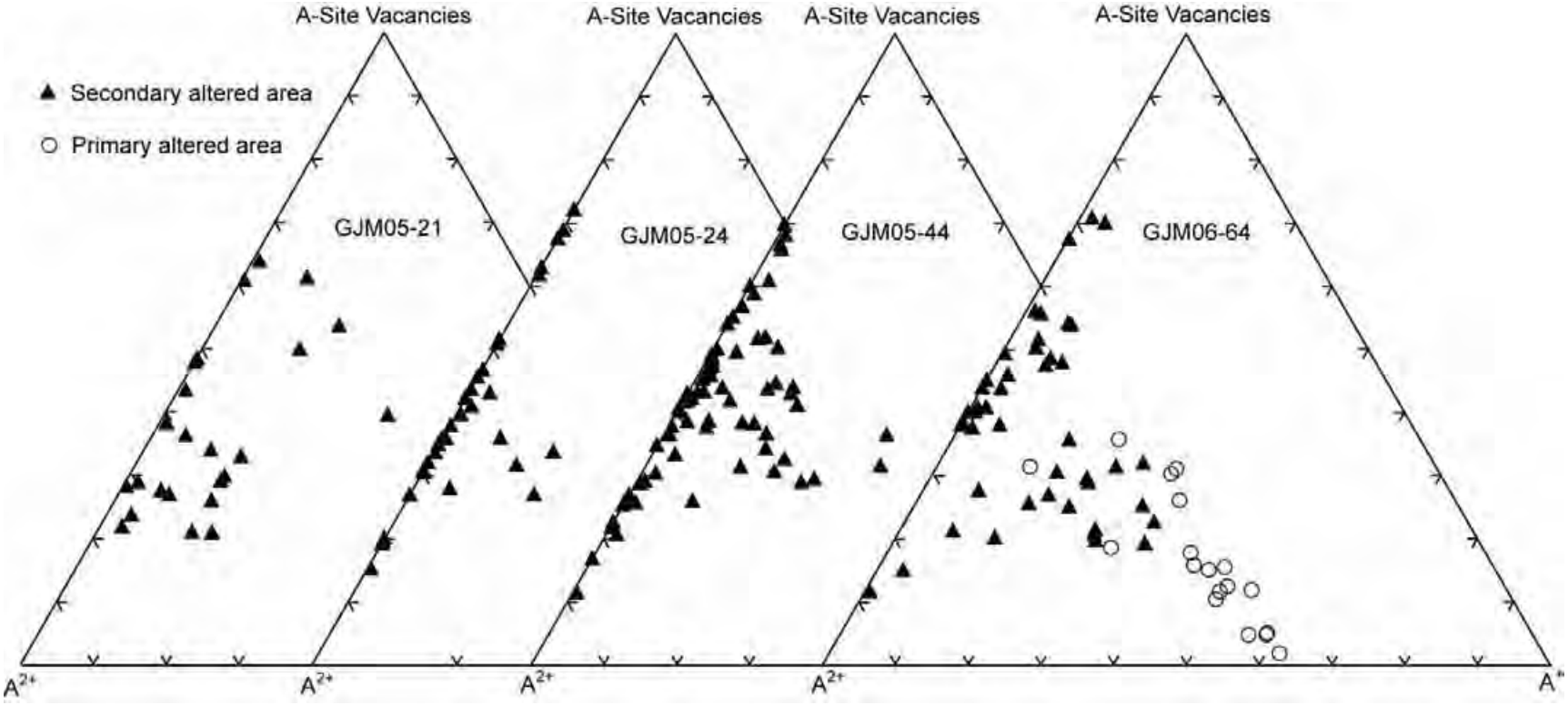
A-Site Vacancies
A-Site Vacancies
A-Site Vacancies
A-Site Vacancies
Secondary altered area
Primary altered area
GJM05-21
GJM05-24
GJM05-44
GJM06-64
A2+
A2+
A2+
A2+
A+